J Mol Model (2013) 19:2355–2361
DOI 10.1007/s00894-013-1776-1

ORIGINAL PAPER

Assessing the accuracy of the general AMBER force field for 2,2,2-trifluoroethanol as solvent

Xiangyu Jia · John Z.H. Zhang · Ye Mei

Received: 17 October 2012 / Accepted: 17 January 2013 / Published online: 10 February 2013

Abstract The alcohol-based cosolvent 2,2,2-trifluoroethanol (TFE) has been used widely in protein science and engineering. Many experimental and computational studies of its impact on protein structure have been carried out, but consensus on the mechanism has not been reached. In the past decade, several molecular mechanical models have been proposed to model the structure and dynamics of TFE. However, further calibration is still necessary. In particular, its compatibility with protein force fields has not been well examined. The general AMBER force field (GAFF) has proved quite successful in modeling small organic molecules, and is compatible with contemporary AMBER force field. In this work, we assessed the accuracy of GAFF for the TFE molecule as a bulk solvent. Several properties, such as density, dipole moment, radial distribution function, etc., were calculated and compared with experimental data. The results show that GAFF plays fairly well in the description of bulk TFE, although there is still room for improvement.

Keywords Trifluoroethanol · Force field · Solvent · Simulation · Permittivity · Dipole

X. Jia · J. Z. Zhang · Y. Mei (✉)
Center for Laser and Computational Biophysics,
State Key Laboratory of Precision Spectroscopy and Department of Physics, Institute of Theoretical and Computational Science,
East China Normal University, Shanghai 200062, China
e-mail: ymei@phy.ecnu.edu.cn

J. Z. Zhang
e-mail: john.zhang@nyu.edu

Present Address:
J. Z. Zhang
Department of Chemistry, New York University,
New York, NY 10003, USA

Introduction

The alcohol-based cosolvent 2,2,2-trifluoroethanol (TFE) has been used widely in the study of protein and peptide structures. At high concentration, TFE tends to denature tertiary hydrophobic interactions in protein and stabilize secondary structures, especially α-helix, in peptides [1–5], while at low concentration it may enhance the stability of protein by an appreciable decrease in the cold denaturation temperature and a modest increase of the hot denaturation temperature [6, 7]. Possible mechanisms by which TFE affects the structure and dynamics of peptides and proteins have been proposed [8]. TFE is a better proton or hydrogen bond donor but a poorer acceptor compared to water, and it is likely to bind preferentially to the main chain carbonyl oxygen group, which leads to enhanced intra-polypeptide hydrogen binding of the amide group. TFE also has a lower dielectric constant as compared to water (27 vs 79) at ambient conditions, which may strengthen long-range electronic interactions. The hydrophobic nature of the CF_3 group may disrupt β-sheet structure but preferentially stabilize helical structures. Some experimental studies [9–11] have been carried out to seek rational explanations for TFE behavior. Hong et al. [12] investigated the alcohol-induced transition about Melittin—a bee venom peptide—and β-lactoglobulin—a predominantly β-sheet protein. The role of several factors was examined, including relative dielectric constant, strength of hydrogen bond and clustering of TEF molecules. Hong et al. [12] found that it was the clustering of TFE molecules rather than the relative dielectric constant or the strength of hydrogen bond that explained the marked effect of TFE. Chagolla et al. [13] explored the conformations of designed peptide Betanova in 42 % trifluoroethanol/water (v/v). They found that although TFE could influence stability in other β-sheet and β-hairpin systems, it failed to influence the relative amounts of conformations of Betanova present in

TFE/water. Therefore a sophisticated and comprehensive understanding of the mechanism remains elusive.

Many experimental and theoretical studies have been carried out to study the properties of TFE as bulk solvent [14–18]. Compared with experiments, computer simulations can provide structural and dynamic information with high spatiotemporal resolution, which is difficult to obtain by experimental means. Popular force fields such as AMBER [19, 20], CHARMM [21], OPLS [22], and GROMOS [23] have been shown to be quite successful in the study of biological molecules. With recent progress in the development of the general amber force field (GAFF) [24, 25] and the CHARMM general force field (CGenFF) [26], these force fields have been extended to general organic molecules for the study of protein/ligand binding systems. Meanwhile, a variety of TFE models have been proposed [27–29]. With these models, some encouraging results have been obtained for proteins and peptides solvated in TFE or TFE/water cosolvent [30, 31]. Berendsen et al. [32] used molecular dynamics (MD) simulations to study the helix stability of the C-terminal part of myoglobin in water with 30 % (v/v) TFE. The GROMOS force field was used to study the parameters of atoms in the TFE molecular except for fluorine the parameters of which were taken from the literature [33, 34]. Their result supported the notion that TFE acts as a structure-forming solvent. Roccatano et al. [35] used their own TFE model [28] to study the stability of three peptides with different secondary structure composition, including Melittin, Betanova and β-hairpin 41–56 from the B1 domain of protein G. They found TFE promoted stability rather than inducing denaturation because it coated the peptide, which promoted the formation of local hydrogen bonds and interacted weakly with nonpolar residues, which indicated that TFE did not severely disrupt hydrophobic interactions within these peptides. Yagisawa et al. [36] used multicanonical molecular dynamics (McMD) to study the 24-residue peptide humanin in TFE/water co-solvent. McMD can sample comprehensive conformations and provide reliable thermodynamic information over a wide temperature range. The results indicated that the helix content and free-energy landscape depended on the solution conditions, and helix induction was a consequence of the preferential solvation. In order to generate a more compatible model with AMBER force field for TFE, in this work we assessed the performance of GAFF in modeling the structural and thermodynamic properties such as density, enthalpy of vaporization, etc., of TFE liquid. The results show that, while there is still room for improvement, GAFF plays fairly well in the description of TFE as bulk solvent.

Methods

The initial structure of TFE was built by GaussView, and then optimized at HF/6-31 G** level using Gaussian 09 [37]. Atomic charges of TFE were fitted according to the dual-step restrained electrostatic potential (RESP) [38–40] method implemented in the AmberTools package [41]. The electrostatic potential on grids around the TFE molecule were calculated at HF/6–31 G* level. The charge scheme quite followed the proposed procedure of GAFF [24, 25] and it was compatible with the AMBER99SB force field [20]. Other parameters, such as bond, angle, dihedral and van der Waals, were taken directly from GAFF. The antechamber module was used to build the parameter set for TFE. The bonded and nonbonded parameters of TFE are listed in Tables 1 and 2, respectively. We then generated a TFE box of 77.2 × 68.6 × 68.4 Å containing 1,715 TFE using the LEaP program in AmberTools 1.5. The whole system was optimized by 4,000 steps of the steepest descent and then by conjugate gradient until convergence was reached. With the volume of the box fixed, this system was heated to 300 K in 100 ps. A 20-ns equilibrium MD simulation under NPT ensemble was carried out to study its physical properties. All bonds involving hydrogen atoms were constrained using the SHAKE [42] algorithm. The integral time step was set to 2 fs. We also tried 1 fs as the integral time step but this made only marginal differences to the calculated physical properties. Therefore all the analysis below is based on the trajectory with a 2-fs time step. The van der Waals interaction was truncated at 10 Å and the periodic electrostatic interaction was calculated by the particle mesh Ewald (PME) [43] algorithm with 10 Å cutoff in real space. The temperature was regulated by employing Langevin dynamics with a collision frequency of 4.0 ps^{-1} and the pressure was regulated using Berendsen's barostat [44]. Simulations were carried out in AMBER 11 [41].

Results

The radial distribution function (RDF) $g(r)$, which is also often referred to as a pair correlation function or pair distribution function, gives the probability of finding a particle in a certain distance r from another particle. RDF provides useful information about the liquid structure, and is related to the potential of mean force, which describes the reversible work for a process in which two tagged particles are moved through the system from infinite separation to a relative separation r and many thermodynamic properties can be obtained from $g(r)$ [45].

The first and second peaks stand for the first and second coordination shell, respectively. The radial distribution function for the carbon atom in the tail group CF_3 [$g_{cc}(r)$] is shown in Fig. 1a. There are several apparent peaks, which indicate the long range of correlation. The locations of peaks and minimums are in agreement with the Roccatano's work [28]. The oxygen–oxygen [$g_{oo}(r)$] and oxygen–hydroxyl

Table 1 Bonded parameters for 2,2,2-trifluoroethanol (TFE)

Bond	RK[a] (kcal mol^{-1} Å^{-2})	REQ[b] (Å)		
CF–F	363.8	1.3440		
CF–CH	303.1	1.5350		
CH–HC	335.9	1.0930		
CH–OH	314.1	1.4260		
OH–HO	369.6	0.9740		
Angle	TK[c] (kcal mol^{-1} rad^{-2})	TEQ[d] (degree)		
F–CF–F	71.260	107.160		
F–CF–CH	66.220	109.410		
CF–CH–HC	46.360	110.070		
CF–CH–OH	67.720	109.430		
HC–CH–OH	50.970	109.880		
HC–CH–HC	39.180	109.550		
CH–OH–HO	47.090	108.160		
Dihedral	IDIVF[e]	PK[f] (kcal mol^{-1})	PHASE[e] (degree)	PN[g]
F–CF–CH–HC	1	0.19	0.0	1
CF–CH–OH–HO	1	0.16	0.0	1
CF–CH–OH–HO	1	0.25	0.0	1
F–CF–CH–OH	9	1.40	0.0	3
HC–CH–OH–HO	3	0.50	0.0	3

[a]Force constant for the bonds of each type

[b]Equilibrium bond length for the bonds of each type

[c]Force constant for the angles of each type

[d]Equilibrium angle for the angles of each type

[e]AMBER parameters used to define the torsional potential energy function

[f]Force constant for the dihedrals of each type

[g]Periodicity of the dihedral of a given type

hydrogen [$g_{oh}(r)$] radial distribution functions in this TFE solvent are shown in Fig. 1b and c respectively, from which the cumulative coordination numbers in the first and second coordination shells are also calculated by

$$n(r) = 4\pi\rho \int_0^r x^2 g(x) dx, \quad (1)$$

where ρ is the number density of TFE molecules. The location of the first peak in $g_{oo}(r)$ is 2.8 Å, which is the distance between the hydroxyl groups in two directly hydrogen-bonded TFE molecules. The second peak in $g_{oo}(r)$ covers a wide range from 3.8 Å to 5.9 Å, and corresponds to the distance between the hydroxyl groups in two TFE molecules hydrogen-bonded to a same TFE molecule, and to neighboring TFE molecules without a hydrogen bond between them. The coordination number of the first shell is 2, and that of the second shell is 4. Long-distance correlation beyond the second coordination shell is very weak, which can be seen from the barely existing third peak. The strong hydrogen-bonding in the first coordination shell can also be confirmed by the location of the first peak (1.8 Å) in the oxygen–hydroxyl hydrogen radial distribution function $g_{oh}(r)$. The second peak in $g_{oh}(r)$ covers a relatively large range from 2.8 Å to 4.0 Å, and it corresponds to the distance between the dangling hydroxyl hydrogen and the hydrogen bond donor in a pair of hydrogen-bonded hydroxyl groups, and the distance between the two hydroxyl groups hydrogen-bonded to a same TFE molecule. The coordination numbers of the first and second coordination shells for $g_{oh}(r)$ are 1 and 2, respectively.

The calculated physical properties, such as density, enthalpy of vaporization, dipole, and heat capacity etc., are shown in Table 3. The experimental measurements are also listed for comparison. These quantities are very important,

Table 2 Nonbonded parameters for TFE

Atom name	Atom type	Charge (*e*)	R[a] (Å)	EDEP[b] (kcal mol^{-1})
F	f	−0.204018	1.7500	0.0610
CF	c3	0.605398	1.9080	0.1094
CH	c3	0.070207	1.9080	0.1094
HC	h1	0.061817	1.3870	0.0157
OH	oh	−0.626284	1.7210	0.2104
HO	ho	0.439100	0.0000	0.0000

[a]van der Waals radius of the atoms

[b]The 6-12 potential well depth

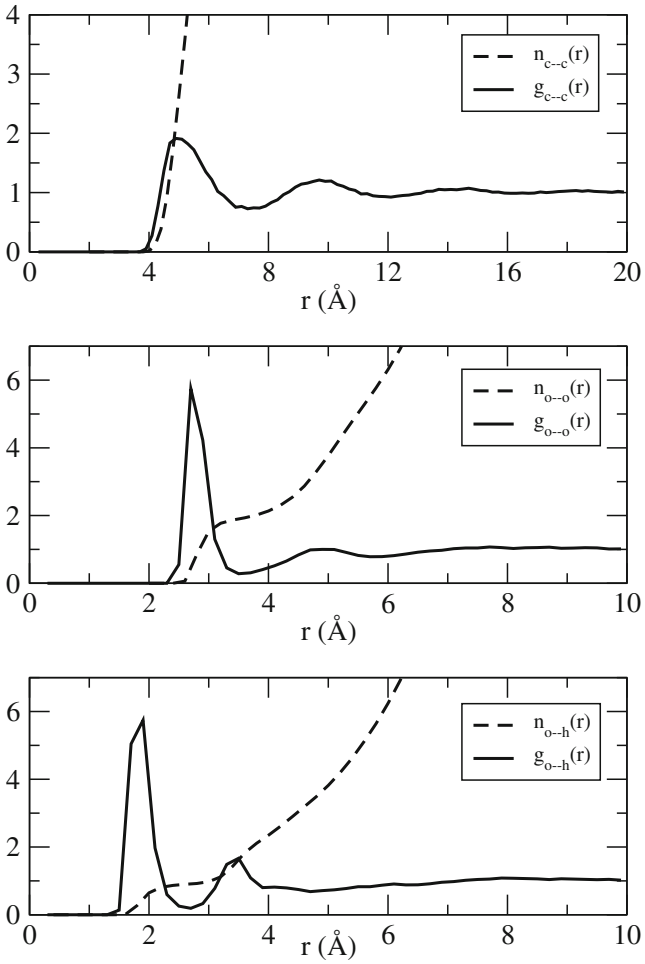

Fig. 1 Radial distribution functions and integrated coordination numbers of **a** C–C, **b** O–O and **c** O–H

and are always investigated when assessing a force field [46]. The average bulk density $\langle\rho\rangle$ is computed from

$$\langle\rho\rangle = \frac{N_{TFE}M_{TFE}}{N_A\langle V\rangle}, \tag{2}$$

in which M_{TFF} is the molecular weight, N_{TFE} is the number of TFE molecules in the system with average volume $\langle V\rangle$, and N_{A} is the Avogadro constant. The volume underwent minor fluctuation during the simulation as shown in Fig. 2. The average volume per TFE was 123.2 Å^3, and the calculated density was 1.348 g/cm^3, which was comparable with the experimental value (1.383 g/cm^3) [47].

Enthalpy of vaporization, also known as the heat of vaporization, is the enthalpy change that occurs during the transition of one mole of substance from the liquid phase to the gas phase, where both of the phases are under equilibrium pressure. The standard way to calculate this quantity is through formula

$$\Delta H_{vap} = H_{gas} - H_{liquid} = E_{gas} - E_{liquid} + P(V_{gas} - V_{liquid}) \tag{3}$$

However, it is practical to employ the ideal gas approximation that the intermolecular interaction energy in gas phase is zero and the molar volume in liquid phase is negligible as compared to that in gas phase. For ideal gas, PV_{gas}approximately equals the product of the gas constant R and the temperature T. Therefore

$$\Delta H_{vap} \approx U_{gas} - E_{liquid} + RT \tag{4}$$

U_{gas} and E_{liquid} can be obtained from the simulations of an isolated TFE and bulk TFE, respectively (see Fig. 3). The calculated enthalpy of vaporization was 44.68 kJ/mol. Comparing to the experimental value (43.97 kJ/mol) [48], the relative error was only 1.6 %.

The only pressure regulation algorithm available in AMBER is the Berendsen's barostat, which is a weak coupling method. It mimics the global energy exchange between the simulated system and an external heat bath in Langevin equation, while local coupling by random noise is eliminated. The fact that this does not reproduce a canonical ensemble [49] and the slow convergence of the second moment [28] made it difficult to calculate values related to the

Table 3 Physical quantities from experiments and molecular dynamics (MD) simulations

	ρ g cm^{-3}	ΔH_{vap} kJ mol^{-1}	μ Debye	D 10^{-9} m^2 s^{-1}	ε	C_p J mol^{-1} K^{-1}	κ_T 10^{-4} bar^{-1}	α_p $10^{-3}K^{-1}$
Experimental	1.383[a]	43.97[b]	2.46[c]	0.60[d]	26.67[e]	177.8[f]	1.0635[g]	1.255[b]
This work	1.348	44.68	2.54	0.28	16.69	269.1	0.8863	1.225

[a] Rochester [47]
[b] Mainar [48]
[c] Mainar [55]
[d] Harris [53]
[e] Mukherjee [57]
[f] Miyana [51]
[g] Patil [50]

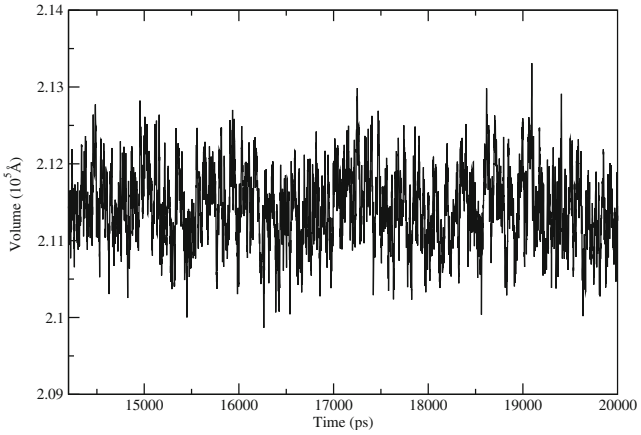

Fig. 2 Time evolution of the volume of the simulated 2,2,2-trifluoroethanol (TFE) box

fluctuation of pressure such as heat capacity, isothermal compressibility and thermal expansion coefficient. On the contrary, the mean value was not sensitive to the method used to mimic an ensemble, and it convergences very rapidly. We can use numerical method to obtain these values from different thermodynamic states [28].

The isothermal compressibility κ_T is defined as

$$\kappa_T = -\frac{1}{V}\left(\frac{\partial V}{\partial p}\right) \approx \left(\frac{ln(\rho_2/\rho_1)}{P_2 - P_1}\right)_T \quad (5)$$

where ρ_1 and ρ_2 were the densities obtained from different simulations using the same temperature but different pressure conditions. The pressure values of P_1 and P_2 were chosen to be 1 bar and 101 bar, respectively. The value obtained was 8.863×10^{-5} bar^{-1}, which is about 17 % lower than the experimental value (1.0635×10^{-4} bar^{-1}) [50].

The thermal expansion coefficient α_p is defined as

$$\alpha_P = \frac{1}{V}\left(\frac{\partial V}{\partial T}\right)_p \approx -\left(\frac{ln(\rho_2/\rho_1)}{T_2 - T_1}\right) \quad (6)$$

Where ρ_1 and ρ_2 are the densities obtained from different simulations using the same pressure but different temperature conditions. Starting from the last frame of the 4 ns simulation at 300 K, we ran another two 20 ns simulations at 290 K and 310 K, respectively; the last 6 ns trajectories were used to calculate ρ_1 and ρ_2. We obtained 1.225×10^{-3} K^{-1} for α_p, which deviated by only 2.4 % from the experimental value ($1.225\times10^{-3}K^{-1}$) [48].

The heat capacity at constant pressure (C_P) was calculated by

$$C_P \approx \left(\frac{H_2 - H_1}{T_2 - T_1}\right)_P. \quad (7)$$

The calculated C_P was 269.1 J mol^{-1} K^{-1}, which was much larger than the experimentally measured value (177.8 J mol^{-1} K^{-1}) [51]. Further calibration of this force field according to the heat capacity is required.

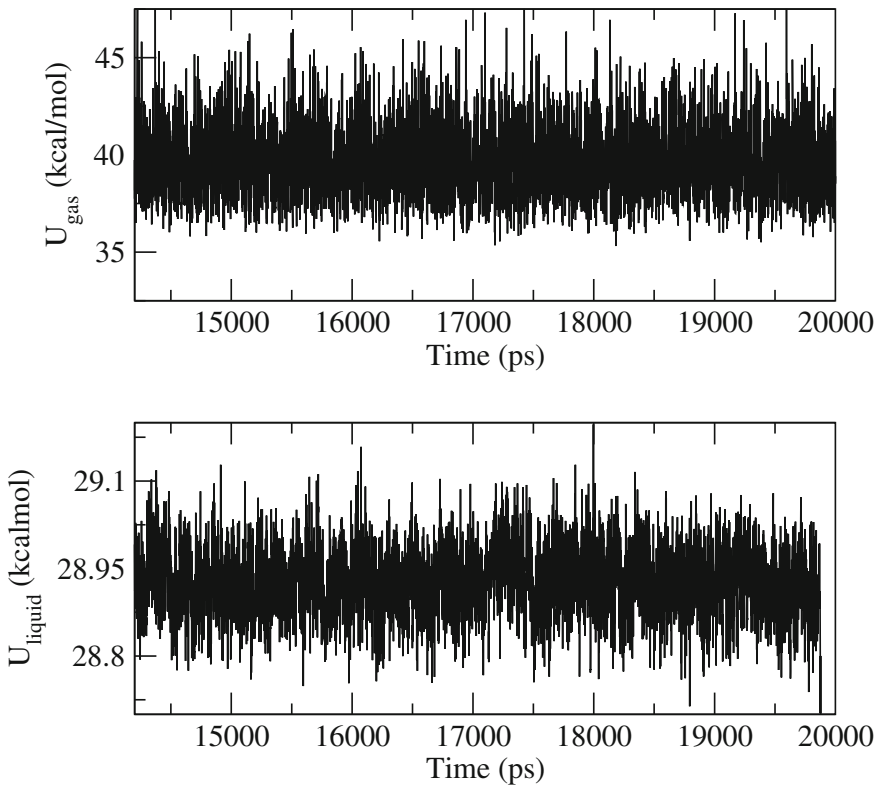

Fig. 3 Time evolutions of potential energies for a single TFE molecule in gas phase (*top*) and in TFE box (*bottom*)

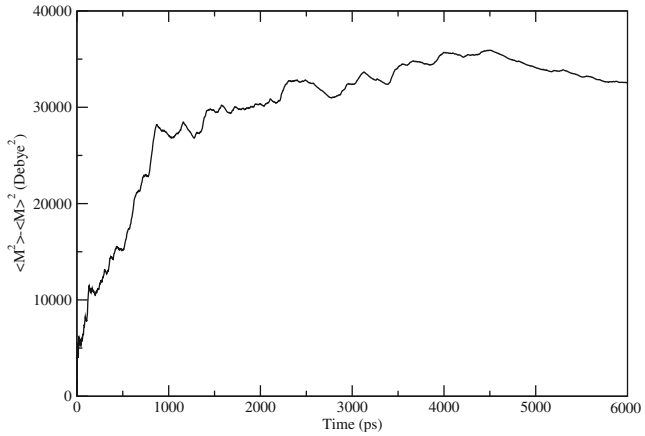

Fig. 4 Time evolution of the fluctuation of the dipole moment of the simulated TFE box

The diffusion coefficient D was obtained from the Einstein equation [52] as

$$D = \lim_{\tau \to \infty} \frac{\left\langle (\mathbf{r}(\mathbf{t}) - \mathbf{r}(\mathbf{0}))^2 \right\rangle}{6t}, \quad (8)$$

where $\mathbf{r}(t)$ is the center of mass (COM) of a TFE molecule at time t. The value obtained was 0.28×10^{-9} m^2 s^{-1}, which is lower than the experimental value (0.6×10^{-9} m^2 s^{-1}) [53]. A lower diffusion coefficient means higher friction coefficient, which reflects collision frequency. VDW interaction is short-range force compared with long-range electrostatic interactions. In the MD simulation of the TFE molecule, the collision frequency is determined mainly by long-range forces; therefore, atomic charges need further refinement. However, it has been found that the computed diffusion constant shows significant system-size dependence with the correction scales as N^{-3}, where N is the number of TFE molecules [54]. Therefore convergence of the diffusion constant requires a large simulation box, which is not applicable to routine simulations.

The magnitude of the dipole moment is an important property that directly determines the strength of TFE–TFE and TFE–protein interactions, and indirectly modulates internal protein interactions. This property can affect the structure of protein by determining the dominant factor between entropy and enthalpy. We calculated the dipole moment of every single TFE molecule in all the frames. The average dipole moment was 2.55 Debye, which was very close to the experimental value (2.46 Debye) [55].

The static relative permittivity is related to the fluctuation of the total dipole moment of the system through [56]

$$(\varepsilon_r - 1)\left(\frac{2\varepsilon_{RF} + 1}{2\varepsilon_{RF} - \varepsilon_r}\right) = \frac{\left\langle \mathbf{M}^2 \right\rangle - \langle \mathbf{M} \rangle^2}{3\varepsilon_0 V k_B T} \quad (9)$$

in which $\mathbf{M}$ is the total dipole moment of the TFE box. The convergence rate of this quantity is very slow, so we collected the last 6 ns simulation data to study its temporal variation. In Fig. 4, the cumulative average of the total dipole moment fluctuation of the system is reported as a function of time. The final value of static relative permittivity was 16.69, which is smaller than the experimental value (26.67) [57], but close to the value calculated by Fioroni [28]. This low static relative permittivity may lead to over-strengthened electrostatic interaction, and this may partly explain the small diffusion constant obtained above.

Conclusions

2,2,2-Trifluoroethanol is used widely in protein science, and has been shown to destabilize tertiary hydrophobic interactions while stabilizing secondary structure. Due to this special feature, it has attracted many experimental and theoretical investigations aimed at revealing the mechanism of its impact on protein structure. The reliability of computer simulation relies on the quality of the force field parameters. The AMBER force field has gained much popularity in the computational biology community. With the development of the general AMBER force field (GAFF), it is now convenient to simulate the interaction between proteins and organic molecules. In this work, we built a TFE box and parameterized the potential utilizing GAFF. MD simulations were carried out to study the structural and thermodynamic properties, such as radial distribution functions, densities, heat of vaporization and dipole, etc. By comparing with experimental measurements, we find the GAFF operates fairly well to delineate the interactions of TFE, especially density, heat of vaporization, dipole and the thermal expansion coefficient. However, other quantities, such as diffusion constant, heat capacity, static relative permittivity and isothermal compressibility, deviate greatly from the true values. Therefore further calibration of the force field is necessary. Possible directions for such refinement are the special treatment for halogen bonds [58, 59] and the implementation of a polarization effect due to the large electron negativity of fluorine atoms.

Acknowledgments We thank the National Natural Science Foundation of China for financial support (Grants No. 10974054, 20933002 and 21173082). We also thank the High Performance Computer Center of East China Normal University for CPU time and support.

References

1. Nelson JW, Kallenbach NR (1986) Proteins 1:211
2. Segawa S-I, Fukuno T, Fujiwara K, Noda Y (1991) Biopolymers 31:497
3. Buck M, Radford SE, Dobson CM (1993) Biochemistry 32:669
4. Jasanoff A, Fersht AR (1994) Biochemistry 33:2129
5. Buck M, Schwalbe H, Dobson CM (1996) J Mol Biol 257:669

6. Martin SR, Esposito V, DeLosRios P, Pastore A, Temussi PA (2008) J Am Chem Soc 130:9963
7. Graziano G (2012) Phys Chem 14:2769
8. Buck M (1998) Q Rev Biophys 31:297
9. Cammers-Goodwin A, Allen TJ, Oslick SL, McClure KF, Lee JH, Kemp DS (1996) J Am Chem Soc 118:3082
10. Vieira EP, Hermel H, Mohwald H (2003) Biochim Biophys Acta 1645:6
11. Benaki D, Zikos C, Evangelou A, Livaniou E, Vlassi M, Mikros E, Pelecanou M (2006) Biochem Biophys Res Commun349:634–642
12. Hong D-P, Hoshino M, Kuboi R, Goto Y (1999) J Am Chem Soc 121:8427
13. Chagolla DP, Gerig JT (2010) Biopolymers 93:893
14. Bako I, Radnai T, Funel MCB (2004) J Chem Phys 121:12472
15. Scharge T, Haber T, Suhm MA (2006) Phys Chem Chem Phys 8:4664
16. Scharge T, Cezard C, Zielke P, Schutz A, Emmeluth C, Suhm MA (2007) Phys Chem Chem Phys 9:4472
17. Yamada Y, Noboru Y, Sakaguchi T, Nibu Y (2012) J Chem Phys 116:2845
18. Burakowski A, Glinski J, Czarnik-Matusewicz B, Kwoka P, Baranowski A, Jerie K, Pfeiffer H, Chatziathanasiou N (2012) J Phys Chem B 116:705
19. Duan Y, Wu C, Chowdhury S, Lee MC, Xiong G, Zhang W, Yang R, Cieplak P, Luo R, Lee T, Caldwell J, Wang J, Kollman P (2003) J Comput Chem 24:1999
20. Hornak V, Abel R, Okur A, Strockbine B, Roitberg A, Simmerling C (2006) Proteins 65:712
21. Brooks BR, Bruccoleri RE, Olafson BD, States DJ, Swaminathan S, Karplus M (1983) J Comput Chem 4:187
22. Kaminski GA, Friesner RA, Tirado-Rives J, Jorgensen WL (2001) J Phys Chem B 105:6474
23. Oostenbrink C, Villa A, Mark AE, van Gunsteren WF (2004) J Comput Chem 25:1656
24. Wang J, Wang W, Kollman PA, Case DA (2006) J Mol Graph Model 25:247
25. Wang J, Wolf RM, Caldwell JW, Kollman PA, Case DA (2004) J Comput Chem 25:1157
26. Vanommeslaeghe K, Hatcher E, Acharya C, Kundu S, Zhong S, Shim J, Darian E, Guvench O, Lopes P, Vorobyov I, Mackerell AD (2010) J Comput Chem 31:671
27. Chitra R, Smith PE (2001) J Chem Phys 115:5521
28. Fioroni M, Burger K, Mark AE, Roccatano D (2000) J Phys Chem B 104:12347
29. Jalili S, Akhavan M (2010) J Comput Chem 31:286
30. Jalili S, Akhavan M (2009) J Theor Comput Chem 08:215
31. Tanizaki S, Clifford J, Connelly BD, Feig M (2008) Biophys J 94:747
32. VanBuuren AR, Berendsen HJC (1993) Biopolymers 33:1159
33. Murto J, Rasanen M, Aspiala A, Lotta T (1984) J Mol Struc Theochem 108:99
34. Radnai T, Ishiguro S, Ohtaki H (1989) J Solut Chem 18:771
35. Roccatano D, Colombo G, Fioroni M, Mark AE (2002) Proc Natl Acad Sci USA 99:12179
36. Yagisawa R, Kamiya N, Ikebe J, Umezawa K, Higo J (2008) Chem Phys Lett 455:293
37. Frisch MJ, Trucks GW, Schlegel HB, Scuseria GE, Robb MA, Cheeseman JR, Scalmani G, Barone V, Mennucci B, Petersson GA, Nakatsuji H, Caricato M, Li X, Hratchian HP, Izmaylov AF, Bloino J, Zheng G, Sonnenberg JL, Hada M, Ehara M, Toyota K, Fukuda R, Hasegawa J, Ishida M, Nakajima T, Honda Y, Kitao O, Nakai H, Vreven T, Montgomery JA Jr, Peralta JE, Ogliaro F, Bearpark M, Heyd JJ, Brothers E, Kudin KN, Staroverov VN, Keith T, Kobayashi R, Normand J, Raghavachari K, Rendell A, Burant JC, Iyengar SS, Tomasi J, Cossi M, Rega N, Millam JM, Klene M, Knox JE, Cross JB, Bakken V, Adamo C, Jaramillo J, Gomperts R, Stratmann RE, Yazyev O, Austin AJ, Cammi R, Pomelli C, Ochterski JW, Martin RL, Morokuma K, Zakrzewski VG, Voth GA, Salvador P, Dannenberg JJ, Dapprich S, Daniels AD, Farkas O, Foresman JB, Ortiz JV, Cioslowski J, Fox DJ (2010) Gaussian 09, Revision B.01. Gaussian, Inc, Wallingford, CT
38. Bayly CI, Cieplak P, Cornell W, Kollman PA (1993) J Phys Chem 97:10269
39. Cornell WD, Cieplak P, Bayly CI, Kollman PA (1993) J Am Chem Soc 115:9620
40. Cieplak P, Cornell WD, Bayly C, Kollman PA (1995) J Comput Chem 16:1357
41. Case DA, Darden TA, Cheatham TE III, Simmerling CL, Wang J, Duke RE, Luo R, Walker R, Zhang W, Merz KM, Wang B, Hayik S, Roitberg A, Seabra G, Kolossvary I, Wong KF, Paesani F, Vanicek J, Liu J, Wu X, Brozell SR, Steinbrecher T, Gohlke H, Cai Q, Ye X, Wang J, Hsieh M-J, Cui G, Roe DR, Mathews DH, Seetin MG, Sagui C, Babin V, Luchko T, Gusarov S, Kovalenko A, Kollman PA (2010) AMBER 11. University of California, San Francisco
42. Ryckaert J-P, Ciccotti G, Berendsen HJC (1977) J Comput Phys 23:327
43. Darden T, York D, Pedersen L (1993) J Chem Phys 98:10089
44. Berendsen HJC, Postma JPM, van Gunsteren WF, DiNola A, Haak JR (1984) J Chem Phys 81:3684
45. Chandler D (1987) Introduction to modern statistical mechanics. Oxford University Press, New York
46. Caleman C, van Maaren PJ, Hong M, Hub JS, Costa LT, van der Spoel D (2012) J Chem Theory Comput 8:61
47. Rochester C, Symonds J (1974) J Fluorine Chem 4:141
48. Mainar AM, Pardo J, Garcia JI, Royo FM, Urieta JS (1998) Faraday Trans 94:3595
49. Morishita T (2000) J Chem Phys 113:2976
50. Patil KJ, Ali SI (1981) Indian J Pure Appl Phys 19:617
51. Miyanaga S, Tamura K, Murakami S (1992) J Chem Thermodyn 24:291
52. Allen MP, Tildesley DJ (1989) Computer simulation of liquids. Clarendon, New York
53. Harris KR, Newitt PJ, Derlacki ZJ (1998) Faraday Trans 94:1963
54. Yeh I-C, Hummer G (2004) J Phys Chem B 108:15873
55. Mainar AM, Pardo J, Royo FM, López M, Urieta JS (1996) J Solut Chem 25:589
56. Neumann M (1983) Mol Phys 50:841
57. Mukherjee LH, Grunwald E (1958) J Phys Chem 62:1311
58. Ibrahim MAA (2012) J Phys Chem B 116:3659
59. Kolar M, Hobza P (2012) J Chem Theory Comput 8:1325